Higgs bosons: Intermediate mass range at e^+e^- colliders

V. Barger,[1] K. Cheung,[2] A. Djouadi,[3] B. A. Kniehl,[4] and P. M. Zerwas[5]
[1] *Physics Department, University of Wisconsin, Madison, WI 53706*
[2] *Department of Physics and Astronomy, Northwestern University, Evanston, Illinois 60208*
[3] *Laboratoire de Physique Nucléaire, Université de Montréal, Case 6128A, Montréal, Québec, Canada H3C 3J7*
[4] *II. Institut für Theoretische Physik, Universität Hamburg, 22761 Hamburg, Germany*
[5] *Deutsches Elektronen-Synchrotron, DESY, 22603 Hamburg, Germany*
(Received 14 June 1993)

We elaborate on the production of the standard model Higgs particle at high-energy e^+e^- colliders through the reaction $e^+e^- \to ZH$. Particular emphasis is put on the intermediate mass range. In addition to the signal we discuss in detail the background processes. Angular distributions which are sensitive to the spin and parity of the Higgs particle are analyzed.

PACS number(s): 14.80.Bn, 13.10.+q

I. THE PHYSICAL BASIS

The fundamental particles in the standard model (SM), gauge bosons, leptons, and quarks, acquire their masses by means of the Higgs mechanism [1]. The masses are generated through the interaction with a nonzero scalar field in the ground state, inducing the spontaneous breaking of the electroweak $SU(2)_I \times U(1)_Y$ symmetry down to the electromagnetic $U(1)_{EM}$ symmetry. To accommodate the well established electromagnetic and weak phenomena, this mechanism requires the existence of at least one weak isodoublet scalar field. The three Goldstone bosons among the four degrees of freedom are absorbed to build up the longitudinal polarization states of the massive $W^\pm, Z$ bosons. One degree of freedom is left over, corresponding to a real physical particle. The discovery of this Higgs particle is the *crucial experiment* for the standard formulation of the electroweak interactions.

The only unknown parameter in the SM Higgs-boson sector is the mass of the Higgs particle. Even though the value of the Higgs-boson mass cannot be predicted, interesting constraints can nevertheless be derived from bounds Λ on the energy range in which the model is taken to be valid before perturbation theory breaks down and new dynamical phenomena could emerge. If the Higgs boson mass is less than about 180 to 200 GeV, the standard model with weakly interacting particles can be extended [2] up the grand unified theory (GUT) scale $\Lambda_{GUT} \sim 10^{16}$ GeV. This attractive idea is very likely to play a key role in the renormalization of the electroweak mixing angle $\sin^2\theta_W$ from the GUT symmetry value 3/8 down to the experimental value ~ 0.2 at low energies. A lower bound on the Higgs boson mass follows in the SM from the requirement of vacuum stability for large top quark masses. If, for a given Higgs boson mass, the top quark mass increases, radiative corrections drive the scalar potential to negative values [3] so that, in turn, for a top mass of ~ 150 GeV, the Higgs boson mass must exceed ~ 100 GeV. We therefore focus in this study on the important Higgs boson mass range $M_Z \le M_H \le 2M_Z$, generically referred to as the intermediate Higgs boson mass range.

Once the Higgs boson mass is fixed, the triple and quartic self-couplings of the SM Higgs particle are uniquely determined. The scale of the Higgs couplings to massive gauge bosons and quarks and/or leptons is set by the masses of these particles. As a result, the profile of the Higgs boson can be predicted completely for a given value of the Higgs mass: the decay properties are fixed and the production mechanisms and rates can be determined.

The width of the SM Higgs particle increases from small values of a few MeV in the 100 GeV mass range quickly to ~ 1 GeV at a mass of $M_H \sim 200$ GeV. Throughout the intermediate mass range, the width remains so small that it cannot be resolved experimentally. The dominant decay mode for masses below ~ 140 GeV is the $b\bar{b}$ decay channel [see Fig. 1]. For higher mass values, the WW and ZZ decays become dominant, one of the vector bosons being virtual below the threshold for two real bosons. Other decay modes [$\tau^+\tau^-, c\bar{c}$, and gg] occur at a level of several percent in the lower part of the intermediate mass range.

The most comprehensive search for Higgs particles has been carried out in Z decays at the CERN e^+e^- collider LEP. A lower bound on the Higgs mass of about $M_H \ge 62.5$ GeV could be established so far [4]; this limit can be raised to ~ 65 GeV by accumulating more statistics. In the second phase of LEP with a total energy of about 180 GeV, Higgs particles can be searched for up to masses of about 80 GeV.

Beyond the LEPII range, new accelerators are needed to search for this particle and to explore its properties. The multi-TeV pp colliders, the CERN Large Hadron Collider (LHC) and Superconducting Super Collider (SSC), can sweep the entire Higgs mass range up to the SM limit of about 800 GeV [5]. In the upper part of the intermediate range, the lepton channels $H \to ZZ^* \to 4l^\pm$ will be used, while in the lower part the rare photon decay $H \to \gamma\gamma$ is the sole decay channel, established so far, which can be exploited to search for

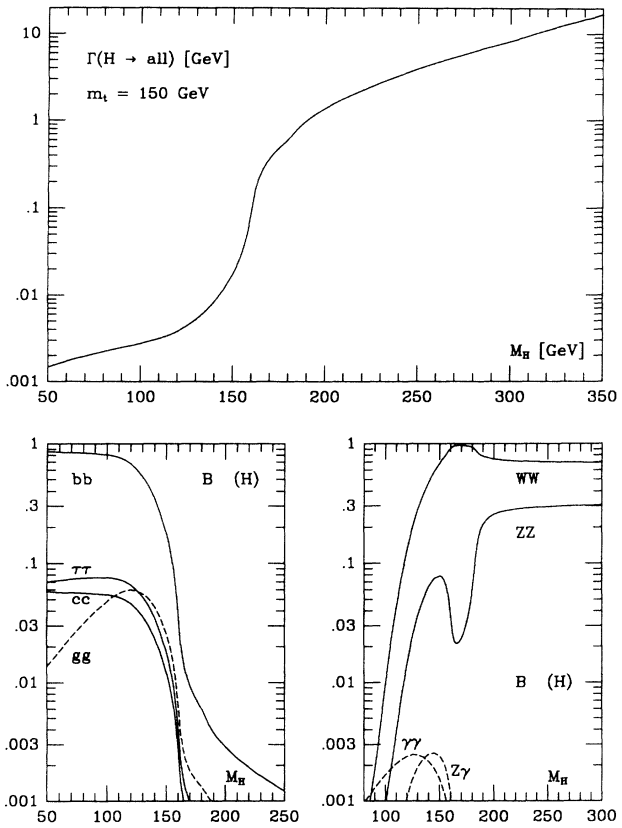

FIG. 1. Update of (a) the total decay width and (b) the decay branching fractions of the Higgs boson in the SM. The top quark mass is assumed to be $m_t = 150$ GeV.

this particle. Because of the overwhelming QCD background, the main decay mode $H \to b\bar{b}$ for $M_H \leq 140$ GeV, nor any mode other than the $\gamma\gamma$ channel, are accessible in hadron colliders. Future e^+e^- colliders, on the other hand, are the ideal machines to investigate the Higgs sector in the intermediate mass range since all major decay modes can be explored, with the Higgs particle produced through several mechanisms [6].

At e^+e^- linear colliders operating in the 300–500 GeV energy range, the main production processes are the WW/ZZ fusion [7] and the bremsstrahlung [8] mechanisms. The cross sections for the fusion mechanisms rise logarithmically with the energy, making these channels dominant at energies ≥ 500 GeV for intermediate mass Higgs bosons. These production channels have been investigated thoroughly in Refs. [9–11]. In the present paper, we analyze in detail the bremsstrahlung process

$$e^+e^- \to Z^* \to Z + H \tag{1}$$

throughout the intermediate mass range [see Fig. 2]. The bremsstrahlung process is dominant for moderate values of the ratio $M_H/\sqrt{s}$, but falls off at high energies according to the scaling law $\sim s^{-1}$. Since this process is fully constrained, missing mass techniques can be applied which allow to search for the Higgs particle without any restrictions on the decay modes. [Higgs events in the ZZ fusion processes $e^+e^- \to e^+e^-(ZZ) \to e^+e^-H$ can also

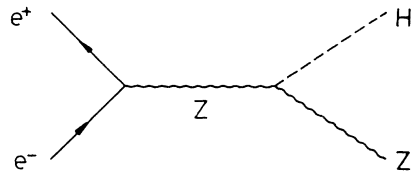

FIG. 2. Feynman diagram for the bremsstrahlung production process $e^+e^- \to HZ$.

be reconstructed completely, yet the production rate is smaller by an order of magnitude.]

Once the Higgs boson is found, it will be very important to explore its properties. This is possible by exploiting the bremsstrahlung process (1). The zero-spin is reflected in the angular distribution [12]. This distribution must approach the $\sin^2\theta$ law asymptotically since, according to the equivalence theorem [13], massive gauge bosons act at high energies like the Goldstone bosons which are absorbed to build up the longitudinal degrees of freedom. The parity can also be studied by analyzing angular correlations. Of tantamount importance is the measurement of the Higgs couplings to gauge bosons and matter particles. The strength of the couplings to Z and W bosons is reflected in the magnitude of the production cross section. The relative strength of the couplings to fermions is accessible through the decay branching ratios. The absolute magnitude is difficult to measure directly. The direct measurement is possible in the small mass window where the Higgs decays to $b\bar{b}$ and WW^* compete with each other; otherwise Higgs bremsstrahlungung off top quarks [14, 15] provides an opportunity to measure the ttH coupling in a limited range of the intermediate mass range. All these couplings grow with the masses of the source particles, a direct consequence of the very nature of the mass generation through the Higgs mechanism. The measurement of these couplings is therefore an important experimental task in the electroweak sector.

The paper is organized as follows. In the next section we shall discuss the production cross section for the bremsstrahlung process including radiative corrections [16]. Depending on the decay modes, various background processes, leading to $Zb\bar{b}$ or ZWW^*, ZZZ^* final states, will be analyzed. We shall also take into account the smearing of the initial state energy due to conventional photon radiation and beamstrahlung [17]. In the third section, we analyze in detail angular distributions and correlations which allow us to verify the J^{PC} quantum numbers of the Higgs particle. Finally we summarize the methods which will allow us to measure the couplings of the Higgs particles to gauge bosons and fermions. No method is known at this time that could be exploited in practice to measure the self-couplings of the SM Higgs field directly [18].

II. BREMSSTRAHLUNG PROCESS OF HIGGS BOSONS

The cross section for the Higgs bremsstrahlung process (1) can be written in a compact form [9],

$$\sigma(ZH) = \frac{G_F^2 M_Z^4}{96\pi s}\,(a_e^2+v_e^2)\,\beta\,\frac{\beta^2+12M_Z^2/s}{(1-M_Z^2/s)^2}\,, \qquad (2)$$

where $a_e=-1, v_e=-1+4\sin^2\theta_W$ are the Z charges of the electron, and $\beta^2=[1-(M_H+M_Z)^2/s][1-(M_H-M_Z)^2/s]$ is the usual two-particle phase space factor, proportional to the momentum squared of the particles in the final state. The cross section is shown in Fig. 3(a) for three energy values 300, 400, and 500 GeV as a function of the Higgs mass, and in Fig. 3(b) for three representative values of the Higgs mass as a function of the total energy $\sqrt{s}$. With $\sigma \sim 200$ fb, a rate of ~ 4000 Higgs particles in the intermediate mass range is produced at an energy $\sqrt{s}=300$ GeV and for an integrated luminosity of $\int \mathcal{L}dt = 20$ fb^{-1} within one year of running. Asymptotically, the cross section scales as s^{-1}.

The radiative corrections *sui generis* [without beamstrahlung] are well under control [16]. The bulk of these corrections is due to photon radiation from the incoming electrons and positrons. The size of the radiative corrections to the total cross section is shown in Figs. 3(a) and 3(b). The solid curves include the one-loop weak corrections and the initial-state radiation up to $O(\alpha^2)$ with the infrared sensitive parts exponentiated. For small M_H they are large and positive since photon radiation pulls the e^+e^- system to smaller energies where the cross section increases. Photon radiation reduces the cross section, on the other hand, when M_H approaches the threshold value. The genuine weak corrections have been shown to be small, reducing the cross section by a few percent [apart from resonating destructive interference spikes at $M_H = 2M_W$ and $2M_Z$].

For narrow-band beam designs such as the Desy-Darmstadt Linear Collider (DLC) and the TeV Energy Superconducting Linear Accelerator (TESLA) [19], beamstrahlung [17] affects the cross section much less than the standard initial-state photon radiation. The change of the cross section, relative to the Born cross section, is exemplified for these design studies in Fig. 4.

The cleanest channel for isolating the signal from the background is provided by the $\mu^+\mu^-/e^+e^-$ decay mode of the Z boson. Depending on the mass of the Higgs boson, either $H \to b\bar{b}$ decays dominate for $M_H \leq 140$ GeV, or $H \to WW^*$ decays for $M_H \geq 140$ GeV. We shall assume a perfect μ-vertex detector with 100% B detection efficiency, which is not far from experimental reality [20]. $Z \to \mu^+\mu^-$ can be tagged by allowing the invariant $\mu^+\mu^-$ mass to vary within $|M_{\mu^+\mu^-} - M_Z| \leq 6$ GeV. For the cases $H \to VV^*$ ($V = W, Z$), we tag the hadronic decays of the on-shell vector boson by requiring that $|M_{jj} - M_V| < M_V/10$. While the signal events prefer the central region of the detector, as discussed later in detail, the background reactions $e^+e^- \to Z + X$ are in general strongly peaked in the forward direction due to the t-channel exchange of electrons [12]. A cut $|\cos\theta_Z| < 0.6$ therefore improves the signal-to-noise ratio significantly. For the study of $H \to b\bar{b}$ the dominant backgrounds come from $e^+e^- \to ZZ^*$, $Z\gamma^*$, $\gamma^*\gamma^* \to (\mu^+\mu^-)(b\bar{b})$, as well as $e^+e^- \to t\bar{t} \to (b\mu^+\nu)(\bar{b}\mu^-\bar{\nu})$. The other back-

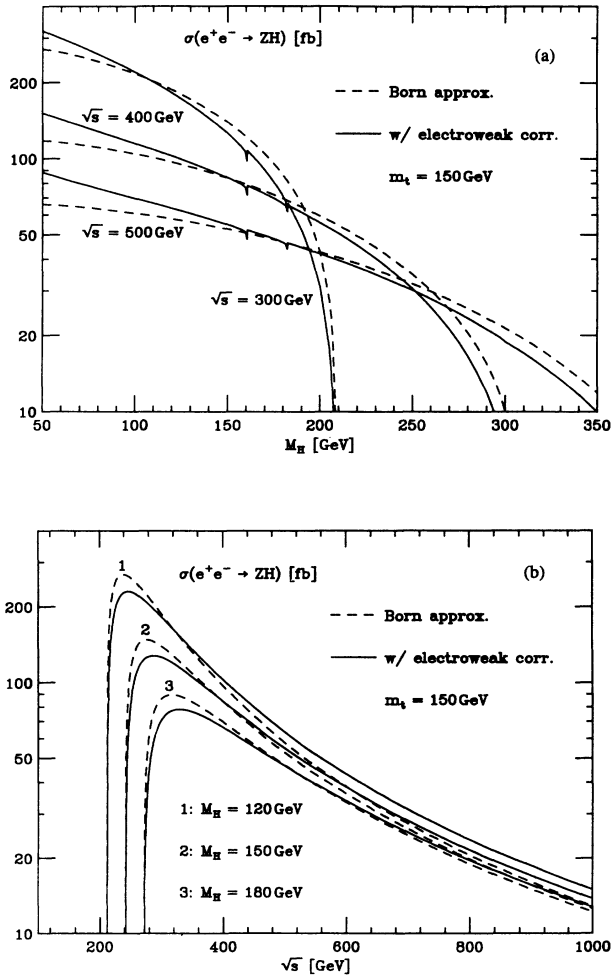

FIG. 3. Total cross sections for the bremsstrahlung process: (a) as a function of the Higgs boson mass and for three energy values $\sqrt{s}=300, 400$, and 500 GeV and (b) as a function of the center-of-mass energy for three values of the Higgs mass $M_H = 120, 150$, and 180 GeV. While the dashed curves represent the cross sections in the Born approximation, the solid curves include the one-loop electroweak corrections assuming $m_t = 150$ GeV.

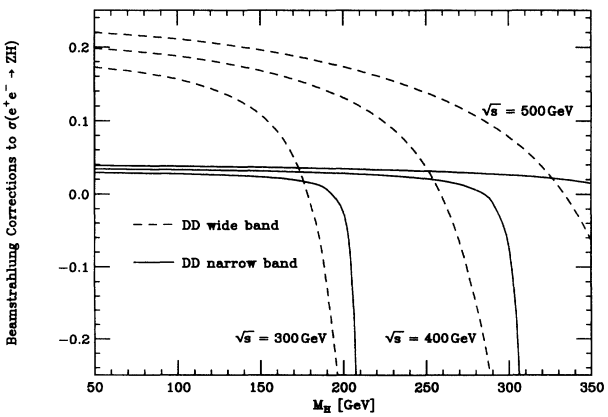

FIG. 4. Beamstrahlung corrections to the $e^+e^- \to ZH$ total cross sections as a function of the Higgs mass and for three energy values $\sqrt{s}=300, 400$, and 500 GeV.

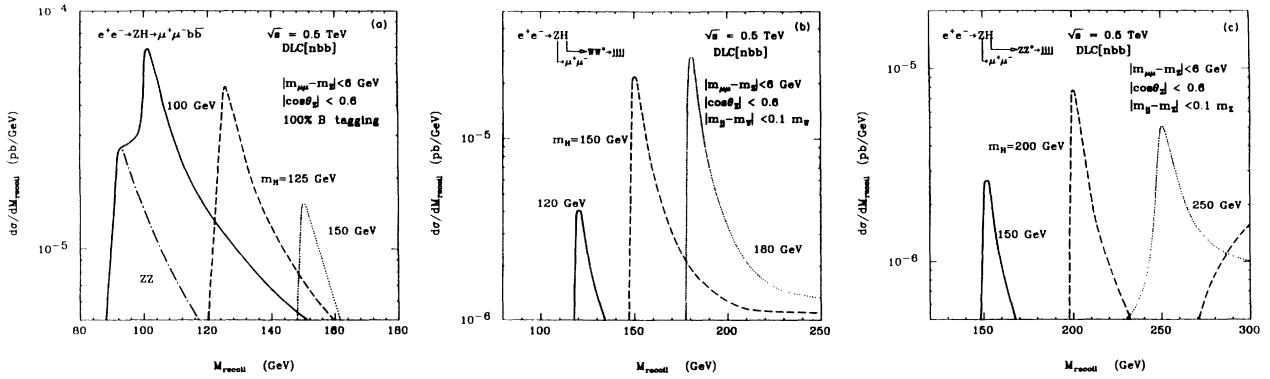

FIG. 5. The missing mass distributions for the $e^+e^- \to \mu^+\mu^- H$ signal as a function of the recoil mass in the three Higgs decay channels (a) $H \to b\bar{b}$ for $M_H = 100, 125$, and 150 GeV, (b) $H \to WW^{(*)}$ for $M_H = 120, 150$, and 180 GeV and (c) $H \to ZZ^{(*)}$ for $M_H = 150, 200$, and 250 GeV. The c.m. energy is fixed to $\sqrt{s} = 500$ GeV and an angular cut $|\cos\theta_{\mu\mu}| < 0.6$ of the $\mu^+\mu^-$ pair momentum with respect to the $e^\pm$ axis has been used; the effects of bremsstrahlung, beamstrahlung, and the beam-energy spread are taken into account.

grounds like $e^+e^- \to b\bar{b}Z$, with the Z bosons radiated off the $b\bar{b}$ final state, are very small and can safely be neglected. On the other hand, for $H \to WW^*$ the dominant background comes from the continuum production of $e^+e^- \to ZWW^* \to (\mu^+\mu^-)+X$. The backgrounds for the channel $H \to ZZ^*$ are more complicated. In addition to the continuum production of $e^+e^- \to ZZZ^*$, there are also combinatorial ambiguities in the signal process from the chain $e^+e^- \to ZH \to (jj)(ZZ^*) \to (jj)(\mu^+\mu^- jj)$, which will not contribute to the Higgs peak in the missing mass spectrum but rather broaden the continuum [see Figs. 5(c) and 6(c)]. Without loss of a large fraction of the signal events, we can assume that all the jets are very well separated, so that the QCD cross section $\sigma(e^+e^- \to q\bar{q}ggZ)$ is of $O(\alpha_W^3\alpha_s^2)$, i.e., suppressed by a factor of $\alpha_W\alpha_s^2$ compared to the signal. The main background reactions are summarized in Table I.

The distributions with respect to the missing mass, $M^2_{\rm recoil} = \left[(p_{e^-} + p_{e^+}) - (p_{\mu^-} + p_{\mu^+})\right]^2$, are shown in Figs. 5(a)–(c) for the three channels defined in Table I assuming $\sqrt{s} = 500$ GeV. In each channel we consider three representative values of M_H: $M_H = 100, 125, 150$ GeV in the $H \to b\bar{b}$ case, $M_H = 120, 150, 180$ GeV in the $H \to WW^*$ case, and $M_H = 150, 200, 250$ GeV in the $H \to ZZ^*$ case. In Figs. 6(a)–(c), we show the corresponding results for $\sqrt{s} = 300$ GeV. Signals and backgrounds have been added, the cuts specified above have been applied, and initial-state bremsstrahlung and beamstrahlung corrections have been taken into account assuming the DLC narrow-band design. For this design, the smearing due to beamstrahlung is small at $\sqrt{s} = 500$ GeV and almost negligible at $\sqrt{s} = 300$ GeV. Without the energy loss connected with these initial-state radiative effects the signals would appear as a sharp peak at $M_{\rm recoil} = M_H$. Throughout our study we have identified jets with the partons in which they originate. In the analysis of the $t\bar{t}$ background we have assumed $m_t = 150$ GeV.

In Figs. 5(a) and 6(a), the $ZH \to (\mu^+\mu^-)(b\bar{b})$ signal is shown with its background added. The $M_{\rm recoil}$ distribution starts slightly below M_H, rises steeply to the peak at M_H, and tails off towards larger values of $M_{\rm recoil}$. For $M_H \leq 100$ GeV, the suppression of the ZZ background by μ vertexing is essential. For larger M_H, the Higgs and Z peaks are clearly separated. Figures 5(b) and 6(b) show the $M_{\rm recoil}$ spectrum for the

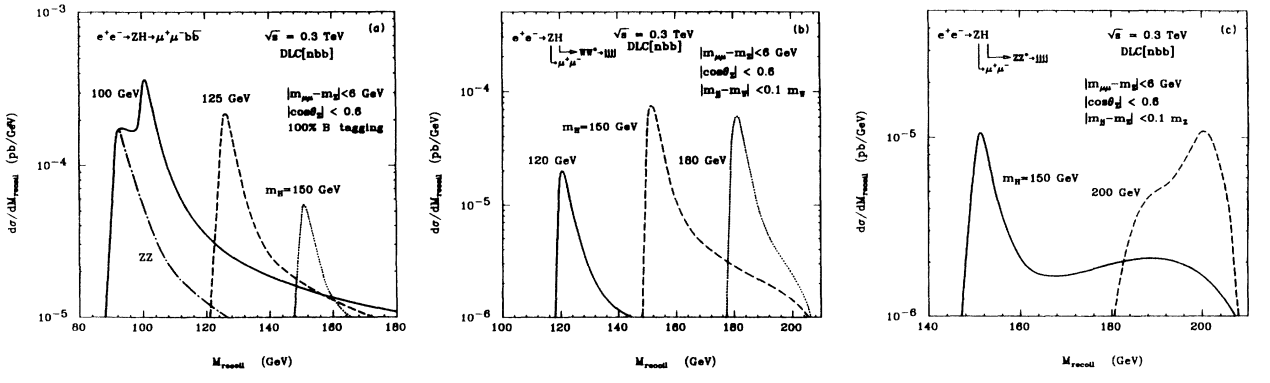

FIG. 6. Same as in Fig. 5 but for $\sqrt{s} = 300$ GeV. Note that there is no $e^+e^- \to t\bar{t}$ background.

TABLE I. Signal and main background processes to Higgs production via bremsstrahlung $e^+e^- \to HZ$, for various mass ranges.

Channel	$H \to b\bar{b}$ $M_H < 160$ GeV	$H \to WW^*$ $M_H > 110$ GeV	$H \to ZZ$ $M_H > 180$ GeV
Signal	$e^+e^- \to (\mu^+\mu^-)(b\bar{b})$	$e^+e^- \to (\mu^+\mu^-)(WW^*)$	$e^+e^- \to (\mu^+\mu^-)(ZZ)$
Bkgd	$e^+e^- \to ZZ, Z\gamma^*, \gamma^*\gamma^*$ $e^+e^- \to t\bar{t} \to b\bar{b}\mu^+\mu^-\nu\bar{\nu}$	$e^+e^- \to ZWW^*$	$e^+e^- \to ZZZ$ $[e^+e^- \to ZH \to (jj)(\mu^+\mu^- jj)]$

$ZH \to (\mu^+\mu^-)WW^*$ signal with the continuum background added. For $M_H = 120$ GeV, the Higgs peak is low due to the small branching fraction of $H \to WW^*$. Once $M_H \geq 140$ GeV, $B(H \to WW^*)$ increases, however, quite fast with M_H [see Fig. 1(b)] and the Higgs peaks are very prominent in the curves for $M_H = 150$ and 180 GeV. All these curves will eventually merge together at the high end of the M_{recoil} spectrum because only the continuum background of $e^+e^- \to ZWW^*$ contributes there. Figures 5(c) and 6(c) exhibit essentially the same features as Figs. 5(b) and 6(b), except that the curves in these figures will not merge at high M_{recoil}. This is due to the presence of the combinatorial "background" from $e^+e^- \to ZH \to (jj)(\mu^+\mu^- jj)$, which will not contribute to the Higgs peak but to the continuum; in particular, the increase of the background at large M_{recoil} for the 200 GeV case is due to combinatorics. In conclusion, M_H can be easily determined from the M_{recoil} spectrum.

At this point, we investigate the significance $S/\sqrt{B}$ of the ZH signal (S) on the ZZ background (B), assuming tagging of one b with probability ϵ_b and misidentification of one c as a b with probability ϵ'_c. In the limit of perfect b tagging, $\epsilon_b = 1$ and $\epsilon'_c = 0$. We neglect the small probability of misidentification of light quarks as b's. Furthermore, we make the following approximations for the branching ratios: $B(H \to b\bar{b}) \gg B(H \to c\bar{c})$ and $B(Z \to b\bar{b}) \approx B(Z \to c\bar{c})$. The probability that at least one of the two b's is detected is $[1-(1-\epsilon_b)^2]$. Thus the significance achieved with at least one b tagged is

$$\frac{S}{\sqrt{B}} = \sqrt{\mathcal{L}}\,\frac{\sigma(ZH)\,B(Z \to \mu^+\mu^-)\,B(H \to b\bar{b})}{\sqrt{2\sigma(ZZ)\,B(Z \to \mu^+\mu^-)\,B(Z \to b\bar{b})}}P_b\,, \tag{3}$$

where $\mathcal{L}$ is the integrated luminosity and

$$P_b = \frac{1-(1-\epsilon_b)^2}{\sqrt{[1-(1-\epsilon_b)^2]+[1-(1-\epsilon'_c)^2]}}\,. \tag{4}$$

The cross sections in fb for the $\mu^+\mu^- b\bar{b}$ final states of ZH and ZZ origin are given in Table II for several values of M_H at $\sqrt{s} = 0.5$ and 0.3 TeV, where the distributions have been integrated over the recoil-mass range $M_H - 5$ GeV $\leq M_{\text{recoil}} \leq M_H + 10$ GeV. Also given is the significance for a luminosity of 10 fb^{-1} assuming perfect b tagging. The values for higher luminosity can be obtained by scaling up these numbers with $\sqrt{\mathcal{L}}$. For a realistic detector it is estimated that $\epsilon'_c \approx 0.2\epsilon_b$ [10]. Using this relation, one has $P_b = 0.54, 0.72, 0.81, 0.86, 0.86$ for $\epsilon_b = 0.2, 0.4, 0.6, 0.8, 0.9$. The reduction in the significance is less than 25% as long as the single-b tagging efficiency is greater than 50%. Under such circumstances, Higgs detection in the $b\bar{b}$ mode of the bremsstrahlung process is feasible at least up to 125 GeV at a 0.5 TeV collider with 10 fb^{-1} luminosity. The situation is even considerably better at $\sqrt{s} = 0.3$ TeV, due to the higher cross section for the signal. Taking into account also $e^+e^- b\bar{b}$ final states, $S/\sqrt{B}$ is scaled up by a factor of $\sqrt{2}$. With double-b tagging, the factor P_b in Eq. (3) is replaced

TABLE II. Cross sections of the $e^+e^- \to ZH \to \mu^+\mu^- b\bar{b}$ signal and the $e^+e^- \to ZZ \to \mu^+\mu^- b\bar{b}$ background, integrated over the range $M_H - 5$ GeV $\leq M_{\text{recoil}} \leq M_H + 10$ GeV, and statistical significance, assuming perfect b tagging and, for the numbers in parentheses, $\epsilon_b = 0.5$ giving $P_b = 0.77$, for $m_H = 100$, 125, 150 GeV and $\mathcal{L} = 10$ and 100 fb^{-1}. The upper entries refer to $\sqrt{s} = 0.5$ TeV, the lower ones to $\sqrt{s} = 0.3$ TeV.

M_H	$\sigma(ZH \to \mu^+\mu^- b\bar{b})$	$\sigma(ZZ \to \mu^+\mu^- b\bar{b})$	$S/\sqrt{B}$	
			10^{-1}fb	100^{-1}fb
100	0.56	0.18	4.1 (3.2)	13.0 (10.1)
	2.53	0.65	9.9 (7.7)	31.4 (24.3)
125	0.42	0.05	5.8 (4.5)	18.4 (14.2)
	1.62	0.15	13.4 (10.4)	42.3 (32.7)
150	0.13	0.03	2.4 (1.8)	7.5 (5.8)
	0.37	0.10	3.7 (2.8)	11.6 (9.0)

by $P_{bb} = \epsilon_b^2/\left(\epsilon_b^2 + \epsilon_c'^2\right)^{1/2}$. Again taking $\epsilon_c' = 0.2\epsilon_b$, one now has $P_{bb} = 0.20$, 0.39, 0.59, 0.78, 0.88 for the same ϵ_b values as above. The requirement of double-b tagging is considerably more costly with low b-tagging efficiency and probably unnecessary, except for confirmation.

III. THE $J^{PC} = 0^{++}$ QUANTUM NUMBERS OF THE HIGGS BOSON

The scalar character of the Higgs particle can be tested at e^+e^- colliders in several ways. The angular distribution of the $e^+e^- \to ZH$ final state depends on the spin and parity of the Higgs particle. The same is true of the angular correlations in the Higgs decay to fermion and gauge boson pairs. The observation of the decay or fusion processes $H \rightleftharpoons \gamma\gamma$ would rule out spin =1 directly by Yang's theorem and fixes the charge conjugation to be positive $C = +$. This follows also from the decay and fusion processes $H \rightleftharpoons ZZ$, as well as from the observation of the bremsstrahlung process $e^+e^- \to Z^* \to ZH$.

A. Production process

Since the production of the final state $e^+e^- \to Z^* \to ZH$ is mediated by a virtual Z boson [transversally polarized along the $e^\pm$ beam axis], the production amplitude could be a monomial in $\cos/\sin\theta$. In the SM, however, the ZZH coupling

$$\mathcal{L}(ZZH) = \left(\sqrt{2}G_F\right)^{1/2} M_Z^2 H Z^\mu Z_\mu \sim G_F^{1/2} H F^{\mu\nu} F_{\mu\nu} \tag{5}$$

is an S-wave coupling $\sim \boldsymbol{\epsilon}_1 \cdot \boldsymbol{\epsilon}_2$ in the laboratory frame, linear in $\sin\theta$ and even under parity and charge conjugation, corresponding to the 0^{++} assignment of the Higgs quantum numbers. The explicit form of the angular distribution is given by

$$\frac{d\sigma(ZH)}{d\cos\theta} \sim \beta^2 \sin^2\theta + 8M_Z^2/s\,. \tag{6}$$

For high energies, the Z boson is produced in a state of longitudinal polarization,

$$\frac{\sigma_L}{\sigma_L + \sigma_T} = 1 - \frac{8M_Z^2}{12M_Z^2 + \beta^2 s}\,, \tag{7}$$

so that, in accordance with the equivalence theorem [13], the production amplitude becomes equal to the amplitude $\mathcal{M}(e^+e^- \to \Phi^0 H)$, with Φ^0 being the neutral Goldstone boson which is absorbed to build up the longitudinal degrees of freedom of the electroweak bosons. The angular distribution therefore approaches the spin-zero distribution asymptotically:

$$\frac{1}{\sigma}\frac{d\sigma(ZH)}{d\cos\theta} \to \frac{3}{4}\sin^2\theta\,. \tag{8}$$

Even though the nature of the Higgs phenomenon requires the Higgs field in the SM to be necessarily a scalar $J^{PC} = 0^{++}$ field, it is nevertheless interesting to confront the predictions in (4,5) with the production

$$e^+e^- \to Z^* \to ZA \tag{9}$$

of a pseudoscalar state $A(0^{-+})$ in order to underline the uniqueness of the SM prediction. The pseudoscalar case is realized in two-doublet Higgs models, in which the ZZA couplings are induced by higher-order loop effects [21]. The effective pointlike coupling

$$\mathcal{L}(ZZA) = \frac{\eta}{4}\left(\sqrt{2}G_F\right)^{1/2} M_Z^2 A Z^{\mu\nu}\widetilde{Z}_{\mu\nu}\,, \tag{10}$$

with η being a dimensionless factor and $\widetilde{Z}^{\mu\nu} = \epsilon^{\mu\nu\rho\sigma}Z_{\rho\sigma}$, is a P-wave coupling, odd under parity and even under charge conjugation. It reduces to $(\boldsymbol{\epsilon}_1 \times \boldsymbol{\epsilon}_2)\cdot(\mathbf{p}_1 - \mathbf{p}_2)$ in the laboratory frame. Since the Z spins are coupled to a vector, the angular distribution is again a binomial in $\sin\theta$:

$$\frac{d\sigma(ZA)}{d\cos\theta} \sim 1 - \frac{1}{2}\sin^2\theta\,, \tag{11}$$

independent of the energy. The Z boson in the final state is purely transversally polarized so that the cross section need not be $\sim \sin^2\theta$ in this case. The total cross section is given by

$$\sigma(ZA) = \eta^2 \frac{G_F^2 M_Z^6}{48\pi M_H^4}\left(a_e^2 + v_e^2\right)\frac{\beta^3}{(1 - M_Z^2/s)^2}\,, \tag{12}$$

where the momentum dependence $\sim \beta^3$ is characteristically different from the ZH production cross section near threshold.

The angular correlations specific to the S-wave 0^{++} Higgs production in $e^+e^- \to ZH$ can directly be confronted experimentally with the process $e^+e^- \to ZZ$. This process has an angular momentum structure that is distinctly different from the Higgs process. Mediated by electron exchange in the t-channel, the amplitude is built-up by many partial waves, peaking in the forward and backward direction. The two distributions are compared with each other in Fig. 7. This figure demonstrates the specific character of the Higgs production process, which

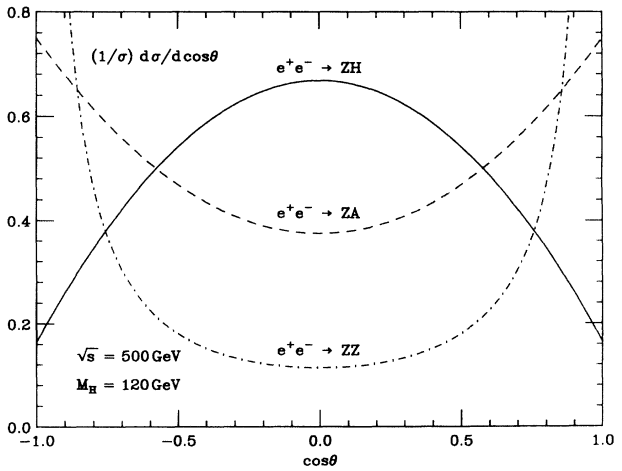

FIG. 7. Angular distributions for the processes $e^+e^- \to ZH$, $e^+e^- \to ZA$ and $e^+e^- \to ZZ$ for a Higgs mass of 120 GeV and a c.m. energy of $\sqrt{s} = 500$ GeV.

is not lost if experimental acceptance cuts and smearing effects are taken into account [10].

Since the longitudinal wave function of a vector boson grows with the energy of the particle, in contrast with the energy independent transverse wave function, the Z boson in the S-wave Higgs production process (1) must asymptotically be polarized longitudinally, Fig. 8. By contrast, the Z bosons from ZA associated production or ZZ pair production are transversally polarized [at high energies in the second case]. This pattern can be checked experimentally. While the distribution of the light fermions in the $Z \to f\bar{f}$ rest frame with respect to the flight direction of the Z [see Fig. 9(a)] is given by $\sin^2\theta_*$ for longitudinally polarized Z bosons, it behaves as $(1 \pm \cos\theta_*)^2$ for transversally polarized states, after averaging over the azimuthal angles. Including the azimuthal angles, the final angular correlations may be written for $e^+e^- \to ZH$ $[Z \to f\bar{f}]$ as

$$\frac{d\sigma(ZH)}{dc_\theta\, dc_{\theta_*}\, d\phi_*} \sim s_\theta^2 s_{\theta_*}^2 - \frac{1}{2\gamma} s_{2\theta} s_{2\theta_*} c_{\phi_*} + \frac{1}{2\gamma^2}[(1+c_\theta^2)(1+c_{\theta_*}^2) + s_\theta^2 s_{\theta_*}^2 c_{2\phi_*}] - \frac{2v_e a_e}{v_e^2+a_e^2}\frac{2v_f a_f}{v_f^2+a_f^2}\frac{2}{\gamma}\left[s_\theta s_{\theta_*} c_{\phi_*} - \frac{1}{\gamma} c_\theta c_{\theta_*}\right], \tag{13}$$

where $s_\theta = \sin\theta$, etc. As before, θ is the polar Z angle in the laboratory frame, θ_* the polar fermion angle in the Z rest frame and ϕ_* the corresponding azimuthal angle with respect to the $e^\pm ZH$ production plane. After integrating out the polar angles θ and θ_*, we find the familiar $\cos\phi_*$ and $\cos 2\phi_*$ dependence associated with $\mathcal{P}$-odd and even amplitudes, respectively,

$$\frac{d\sigma(ZH)}{d\phi_*} \sim 1 + a_1 \cos\phi_* + a_2 \cos 2\phi_*\,, \tag{14}$$

with

$$a_1 = -\frac{9\pi^2}{32}\frac{\gamma}{\gamma^2+2}\frac{2v_e a_e}{v_e^2+a_e^2}\frac{2v_f a_f}{v_f^2+a_f^2}\,, \qquad a_2 = \frac{1}{2}\frac{1}{\gamma^2+2}\,. \tag{15}$$

The azimuthal angular dependence disappears for high energies $\sim 1/\gamma$ as a result of the dominating longitudinal polarization of the Z boson.

Note again the characteristic difference to the pseudoscalar 0^{-+} case $e^+e^- \to ZA$ $[Z \to f\bar{f}]$,

$$\frac{d\sigma(ZA)}{dc_\theta dc_{\theta_*} d\phi_*} \sim 1 + c_\theta^2 c_{\theta_*}^2 - \frac{1}{2}s_\theta^2 s_{\theta_*}^2 - \frac{1}{2}s_\theta^2 s_{\theta_*}^2 c_{2\phi_*} + 2\frac{2v_e a_e}{v_e^2+a_e^2}\frac{2v_f a_f}{v_f^2+a_f^2} c_\theta c_{\theta_*}\,. \tag{16}$$

This time the azimuthal dependence is P even and independent of the energy in contrast to the 0^{++} case; after integrating out the polar θ, θ_* angles,

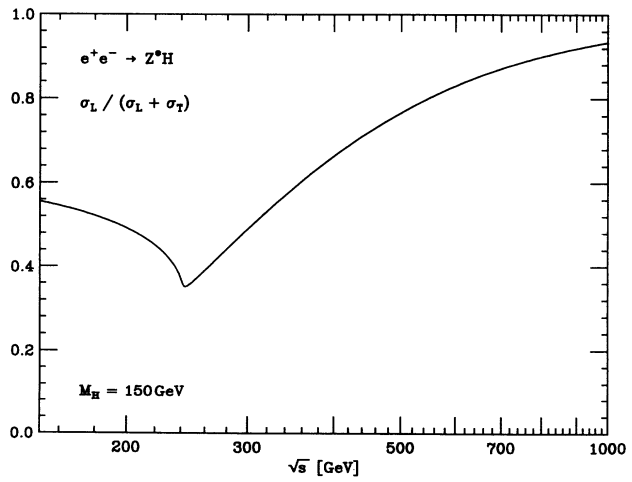

FIG. 8. Cross sections for the production of longitudinal vector bosons normalized to the total cross sections for the processes $e^+e^- \to ZH$ as a function of the c.m. energy for $M_H = 150$ GeV.

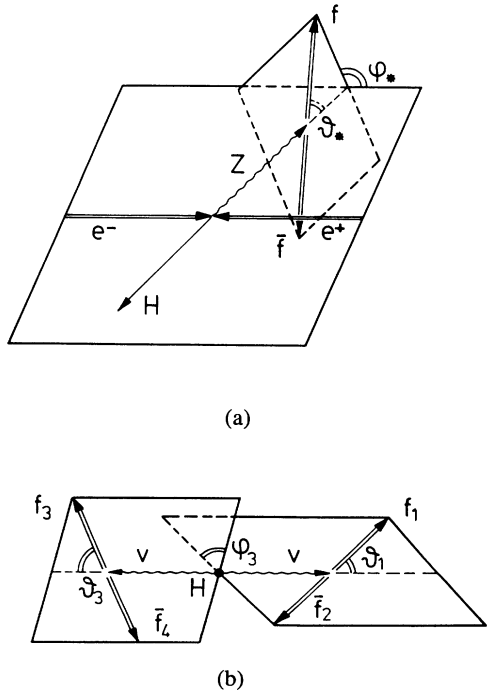

FIG. 9. Definition of the polar and azimuthal angles (a) in the production process $e^+e^- \to HZ$ $[Z \to f\bar{f}]$, and (b) in the decay processes $H \to VV^{(*)} \to (f_1\bar{f}_2)(f_3\bar{f}_4)$.

$$\frac{d\sigma(ZA)}{d\phi_*} \sim 1 - \frac{1}{4}\cos 2\phi_* \,. \tag{17}$$

We can thus conclude that the angular analysis of the Higgs production in $e^+e^- \to Z^* \to ZH$ $[Z \to f\bar{f}]$ allows stringent tests of the $\mathcal{J}^{\mathcal{PC}} = 0^{++}$ quantum numbers of the Higgs boson. This is a direct consequence of the 0^{++} coupling $\epsilon_1 \cdot \epsilon_2$ of the ZZH vertex in the production amplitude.

B. Decay processes

The zero-spin of the Higgs particle can be checked directly through the lack of any angular correlation between the initial and final state particles [10]. In the following discussion we shall concentrate on Higgs boson decays to vector bosons $V = W, Z$, which will provide us with signatures similar to those studied in the previous section, including the discrimination between 0^{++} and 0^{-+} decays. The analysis applies in a straightforward way to Higgs particles in the e^+e^- environment. Background problems require a more sophisticated discussion for Higgs particles produced at the SSC and LHC. Since some of the material on this method had been worked out before [22], we focus on novel points which have not been elaborated in detail so far.

Above the $H \to WW$ and ZZ decay thresholds, the partial width into massive gauge boson pairs may be written as [23]

$$\Gamma(H \to VV) = \delta_V \frac{\sqrt{2}G_F}{32\pi} M_H^3 (1 - 4x + 12x^2)\beta \,, \tag{18}$$

where $x = M_V^2/M_H^2$, $\beta = \sqrt{1-4x}$ and $\delta_V = 2(1)$ for $V = W(Z)$. For large Higgs masses, the vector bosons are longitudinally polarized [see Fig. 10],

$$\frac{\Gamma_L}{\Gamma_L + \Gamma_T} = \frac{1 - 4x + 4x^2}{1 - 4x + 12x^2} \,, \tag{19}$$

while the L, T polarization states are democratically populated near the threshold, at $x = 1/4$. The HZZ coupling $\epsilon_1 \cdot \epsilon_2$ is the same S-wave coupling which we have discussed earlier. Since the longitudinal wave functions are linear in the energy, the width grows as the third power of the Higgs mass. The electroweak radiative corrections [24] are positive and amount to a few percent above the threshold.

Below the threshold for two real bosons, the Higgs particle can decay into real and virtual VV^* pairs, primarily WW^* pairs above $M_H \sim 110$ GeV. The partial decay width, W charges summed over, is given [25] by

$$\Gamma(H \to VV^*) = \frac{3G_F^2 M_V^4}{16\pi^3} M_H R(x) \delta_V' \,, \tag{20}$$

with $\delta_W' = 1$ and $\delta_Z' = 7/12 - 10\sin^2\theta_W/9 + 40\sin^4\theta_W/27$ and

$$R(x) = \frac{3(1 - 8x + 20x^2)}{(4x-1)^{1/2}} \arccos\left(\frac{3x-1}{2x^{3/2}}\right) - \frac{1-x}{2x}(2 - 13x + 47x^2) - \frac{3}{2}(1 - 6x + 4x^2)\ln x \,. \tag{21}$$

The invariant mass (M_*) spectrum of the off-shell vector boson peaks close to the kinematical maximum corresponding to zero momentum of the on- and off-shell vector bosons in the final state [see Fig. 11]:

$$\frac{d\Gamma}{dM_*^2} = \frac{3G_F^2 M_V^4}{16\pi^3 M_H} \delta_V' \frac{\beta(M_H^4\beta^2 + 12M_V^2 M_*^2)}{(M_*^2 - M_V^2)^2 + M_V^2\Gamma_V^2} \,, \tag{22}$$

where $\beta^2 = [1 - (M_V + M_*)^2/M_H^2]\ [1 - (M_V - M_*)^2/M_H^2]$. Since both V and V^* preferentially have small momenta, the transverse and longitudinal polarization states are populated with almost equal probabilities:

$$\frac{d\Gamma_L/dM_*^2}{d\Gamma/dM_*^2} = 1 - \frac{8M_V^2 M_*^2}{M_H^4\beta^2 + 12M_V^2 M_*^2} \,. \tag{23}$$

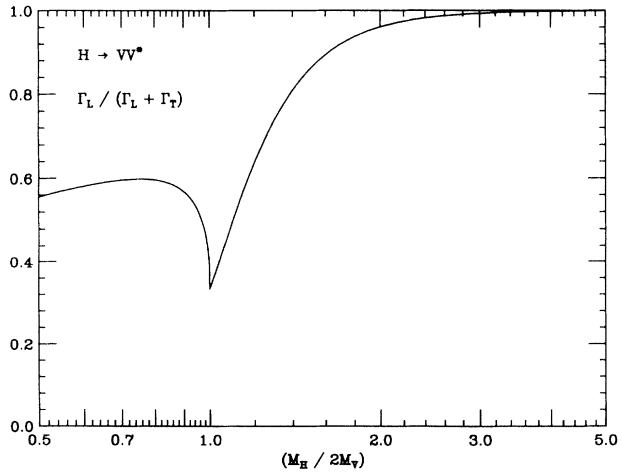

FIG. 10. The width of Higgs decays to longitudinally polarized vector bosons normalized to the total width for the decays $H \to VV^{(*)}$ as a function of the mass ratio $M_H/(2M_V)$.

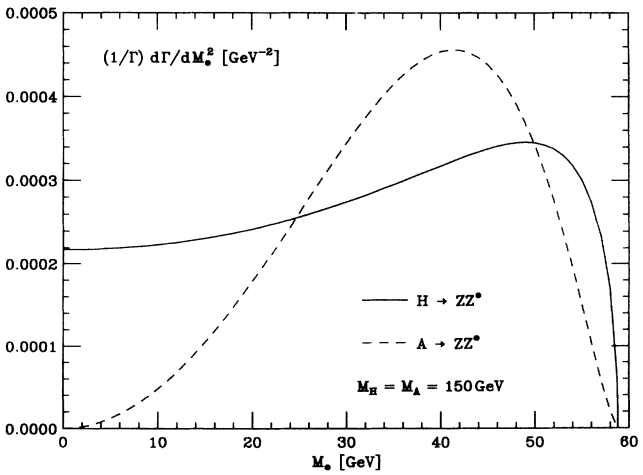

FIG. 11. The distributions with respect to the invariant mass of the off-shell vector bosons in the decay processes $H \to ZZ^*$ and $A \to ZZ^*$ for $M_H = M_A = 150$ GeV.

Neglecting the widths of the vector bosons, Γ_V, we find, after summing over all M_* values [see Fig. 10],

$$\frac{\Gamma_L}{\Gamma_L+\Gamma_T} = \frac{R_L(M_V^2/M_H^2)}{R(M_V^2/M_H^2)}, \tag{24}$$

where R is given in Eq. (19) and

$$\begin{aligned} R_L(x) = {} & \frac{3-16x+20x^2}{(4x-1)^{1/2}} \arccos\left(\frac{3x-1}{2x^{3/2}}\right) \\ & -\frac{1-x}{2x}(2-13x+15x^2) \\ & -\frac{1}{2}(3-10x+4x^2)\ln x\,. \end{aligned} \tag{25}$$

The angular distributions of the fermions in the 0^{++} decay process

$$H \to V\,V^* \to (f_1\bar{f}_2)\;(f_3\bar{f}_4) \qquad [V=W,Z] \tag{26}$$

are quite similar to the rules found for the production process. Denoting polar and azimuthal angles of the fermions f_1, f_3 in the rest frames of the vector bosons by $(\theta_1, 0)$ and (θ_3, ϕ_3), respectively, [see Fig. 9(b)] the angular distributions for the scalar case are given by

$$\begin{aligned} \frac{d\Gamma(H\to VV^*)}{dc_{\theta_1}dc_{\theta_3}d\phi_3} \sim {} & s^2_{\theta_1}s^2_{\theta_3} + \frac{1}{2\gamma_1\gamma_3(1+\beta_1\beta_3)}s_{2\theta_1}s_{2\theta_3}c_{\phi_3} + \frac{1}{2\gamma_1^2\gamma_3^2(1+\beta_1\beta_3)^2}[(1+c^2_{\theta_1})(1+c^2_{\theta_3}) + s^2_{\theta_1}s^2_{\theta_3}c_{2\phi_3}] \\ & - \frac{2v_1a_1}{v_1^2+a_1^2}\frac{2v_3a_3}{v_3^2+a_3^2}\frac{2}{\gamma_1\gamma_3(1+\beta_1\beta_3)}\left[s_{\theta_1}s_{\theta_3}c_{\phi_3} + \frac{1}{\gamma_1\gamma_3(1+\beta_1\beta_3)}c_{\theta_1}c_{\theta_3}\right]. \end{aligned} \tag{27}$$

For $V=W$, the charges are $v_i = a_i = 1$; for $V=Z$, $v_i = 2I_{3i} - 4e_i\sin^2\theta_W$ and $a_i = 2I_{3i}$. β_i, γ_i are the velocities and γ factors of the [on- and/or off-shell] vector bosons. As expected, the dependence on the azimuthal angle between the decay planes disappears for large Higgs masses, a consequence of the asymptotic longitudinal V polarization. After integrating out the polar angles, we are left with

$$\frac{d\Gamma(H\to VV^*)}{d\phi_3} \sim 1 + a_1\cos\phi_3 + a_2\cos 2\phi_3\,, \tag{28}$$

where

$$\begin{aligned} a_1 &= -\frac{9\pi^2}{32}\frac{\gamma_1\gamma_3(1+\beta_1\beta_3)}{\gamma_1^2\gamma_3^2(1+\beta_1\beta_3)^2+2}\frac{2v_1a_1}{v_1^2+a_1^2}\frac{2v_3a_3}{v_3^2+a_3^2}, \\ a_2 &= \frac{1}{2}\frac{1}{\gamma_1^2\gamma_3^2(1+\beta_1\beta_3)^2+2}. \end{aligned} \tag{29}$$

The coefficient a_1 measures the $\mathcal{P}$-odd amplitude.

Both the azimuthal angular correlations as well as the distributions of the polar angles are sensitive to the spin-parity assignments of the Higgs particle, which affect strongly the populations of the W, Z polarization states. We will study this point by confronting again the scalar $H(0^{++})$ decay with the pseudoscalar $A(0^{-+})$ decay distributions:

$$A \to V\,V^* \to (f_1\bar{f}_2)\;(f_3\bar{f}_4) \qquad [V=W,Z]. \tag{30}$$

For the $AV_{\mu\nu}\tilde{V}^{\mu\nu}$ coupling defined before, the angular distribution is given by

$$\begin{aligned} \frac{d\Gamma(A\to VV^*)}{dc_{\theta_1}dc_{\theta_3}d\phi_3} \sim {} & 1 + c^2_{\theta_1}c^2_{\theta_3} - \frac{1}{2}s^2_{\theta_1}s^2_{\theta_3} - \frac{1}{2}s^2_{\theta_1}s^2_{\theta_3}c_{2\phi_3} \\ & - 2\frac{2v_1a_1}{v_1^2+a_1^2}\frac{2v_3a_3}{v_3^2+a_3^2}c_{\theta_1}c_{\theta_3}\,. \end{aligned} \tag{31}$$

The normalization follows from the total and differential widths,

$$\Gamma(A\to VV^*) = \frac{3G_F^2M_V^6}{8\pi^3M_A}\delta_V'\eta^2 A\left(\frac{M_V^2}{M_A^2}\right) \tag{32}$$

with

$$\begin{aligned} A(x) = {} & (1-7x)(4x-1)^{1/2}\arccos\left(\frac{3x-1}{2x^{3/2}}\right) \\ & -\frac{1-x}{6}(17-64x-x^2) \\ & +\frac{1}{2}(1-9x+6x^2)\ln x\,, \end{aligned}$$

and

$$\frac{d\Gamma(A\to VV^*)}{dM_*^2} = \frac{3G_F^2M_V^6}{8\pi^3M_A}\delta_V'\eta^2\frac{M_*^2\beta^3}{(M_*^2-M_V^2)^2+M_V^2\Gamma_V^2}, \tag{33}$$

where M_* denotes the mass of the off-shell vector boson. The M_* spectra for $H\to Z^*Z$ and $A\to Z^*Z$ are shown in Fig. 11 assuming $M_H = M_A = 150$ GeV. The mass and momentum dependence of the width are determined by the P wave decay characteristics and the transverse polarization of the vector bosons. In the same way, the angular distributions [which are independent of the masses] reflect the transverse W, Z polarizations.

For Higgs masses below 140 GeV, the dominant decay mode are $b\bar{b}$ decays. A fraction of a few percent decay into $\tau^+\tau^-$ final states. For moderate to large tgβ values, these are also the main decay modes for scalar and pseudoscalar Higgs particles in the minimal supersymmetric extension of the standard model (MSSM). While the zero spin can again be checked experimentally by the lack of any correlations between the final and initial state particles, it is quite difficult to verify the $\pm$ parity of the

states in the decay distributions. This information must be extracted from correlations between the b and $\bar{b}$, τ^- and τ^+ spin components in the planes transverse to the $b\bar{b}$ and $\tau^+\tau^-$ axes:

$$\text{scalar/pseudoscalar} \; : \; C = 1 - s^f_{||} s^{\bar{f}}_{||} \pm s^f_{\perp} s^{\bar{f}}_{\perp} \; .$$

The spin correlations are reflected in correlations between the f and $\bar{f}$ decay products [26]. Depolarization effects through $b, \bar{b}$ fragmentation into pseudoscalar B mesons [27] introduce systematic uncertainties into this channel which are very hard to control, so that the rare but clean $\tau\tau$ final states are the proper instrument to study this problem.

At e^+e^- colliders, the parity of the Higgs bosons in the MSSM can be studied in the following way.

(i) Since the scalar MSSM Higgs particles h, H couple to vector bosons directly, the positive parity can be checked by analyzing the Z final states in $e^+e^- \to Z^* \to ZH$ $[Z \to f\bar{f}]$ as discussed above in great detail. This method is equivalent to the analysis of the $h, H \to VV$ decays.

(ii) The fusion of Higgs particles by linearly polarized photon beams depends on the angle between the polarization vectors [28]. For scalar particles the production amplitude $\sim \boldsymbol{\epsilon}_1 \cdot \boldsymbol{\epsilon}_2$ is nonzero only for parallel vectors while pseudoscalar particles with amplitudes $\sim \boldsymbol{\epsilon}_1 \times \boldsymbol{\epsilon}_2$ require perpendicular polarization vectors. For typical experimental setups for Compton backscattering of laser light [29], the maximum degree of linear polarization of the generated hard photon beams is less than about 30% so that the efficiency for two polarized beams is reduced to less than 10% [30]. This method therefore requires high luminosities, and, moreover, a careful analysis of background rejection due to the enormous number of $b\bar{b}$ pairs produced in $\gamma\gamma$ collisions [31].

IV. SUMMARY

In this report we have described the production of Higgs particles in the intermediate mass range and the analysis of their $\mathcal{J}^{\mathcal{PC}}$ assignment. Even though we have focused on e^+e^- linear colliders, certain elements of our study on Higgs decays are also relevant to Higgs particles eventually produced at the proton colliders SSC and LHC.

It has been shown that the search for SM Higgs particles in the intermediate mass range is easy at e^+e^- colliders since the signal sticks out of the background processes very clearly. μ-vertexing of the b quarks will be essential for Higgs bosons in the Z-mass range. The significance of the ZH signal will only reduce by 25% when at least one b is tagged with an efficiency of 50% per b. With 50 fb^{-1} luminosity and a b-tagging efficiency of $\epsilon_b = 0.5$, a Higgs boson of mass 100–150 GeV could be detected with a significance $S/\sqrt{B}$ greater than 4.1 (6.3) at $\sqrt{s} = 500$ (300) GeV. Above 110 GeV, and in particular beyond 140 GeV, the Higgs decay channels into electroweak vector-boson pairs can be exploited. As discussed previously [11], the potential for the discovery of heavy Higgs bosons may be augmented by taking the WW-fusion process into account. At $\sqrt{s} = 0.5$ TeV and 50 fb^{-1}, the $\nu\bar{\nu}H \to \nu\bar{\nu}WW(ZZ) \to \nu\bar{\nu}jjjj$ signal and its total background have $S/\sqrt{B} = 6.8$ (2.4) for $M_H = 300$ (350) GeV, without the use of b tagging to identify the dominant $t\bar{t}$ background.

The spin and parity assignments can, on one hand, be checked easily in Higgs decays to vector boson pairs. Angular correlations among the lepton and/or quark decay products reflect their polarization states, primarily longitudinal or democratic for large or moderate Higgs masses, respectively, if $\mathcal{J}^{\mathcal{PC}} = 0^{++}$, and transverse if $\mathcal{J}^{\mathcal{PC}} = 0^{-+}$. This information can also be extracted, on the other hand, from the angular behavior of the $e^+e^- \to ZH$ production process. The parity analysis of pseudoscalar Higgs particles, in supersymmetric extensions of the standard model for instance, requires difficult measurements of the fermionic decay states, or polarization analyses in the case of $\gamma\gamma$ fusion.

In addition to the spin-parity assignments, the essential nature of the SM Higgs particle must be established by demonstrating that couplings to other fundamental particles grow with their masses. Even though we did not analyze these couplings in detail, a few remarks ought to be added to round off the discussion [9]. The Higgs couplings to massive gauge bosons can directly be determined from the measurement of the production cross sections: the HZZ coupling in the bremsstrahlung and in the ZZ fusion processes; the HWW coupling in the WW fusion process. For sufficiently large Higgs masses above ~ 250 GeV, these couplings can also be determined experimentally from the decay widths $H \to ZZ, WW$. Higgs couplings to fermions are not easy to measure directly. For Higgs bosons in the intermediate mass range where the decays into $b\bar{b}, c\bar{c}$ and $\tau^+\tau^-$ are important, the decay width is so narrow that it cannot be resolved experimentally. Nevertheless, the branching ratios into τ leptons and charm quarks reveal the couplings of these fermions relative to the coupling of the b quarks into which the Higgs boson decays predominantly. In the upper part of the intermediate mass range but below the threshold for real WW decays, the branching ratio $B(H \to WW^*)$ is sizeable and can be determined experimentally [32]. In this case, the absolute values of the b and eventually of the c, τ couplings can be derived once the HZZ/HWW couplings are fixed by the production cross sections. The decays $H \to gg$ and $\gamma\gamma, Z\gamma$ and the fusion processes $gg, \gamma\gamma \to H$ are mediated by loop diagrams and they are proportional to the couplings of the Higgs boson to heavy particles. The number of heavy particles can be counted in these processes if their masses are generated by the Higgs mechanism and their couplings to the Higgs particles grow with the mass. [This is not the case for heavy supersymmetric particles which decouple asymptotically from the HVV vertices.] In the standard model only the top quark contributes to the Hgg vertex so that the Htt coupling can be measured in the gluonic decays of the Higgs particle [and, in the same way, through the cross section for the gluon fusion $gg \to H$ at hadron colliders]. In the case of $H \to \gamma\gamma, Z\gamma$ additional contributions to the decay amplitudes come

from W loops. A direct way to determine the Yukawa coupling of the intermediate mass Higgs boson to the top quark in the range $m_H \leq 120$ GeV are provided by the bremsstrahlung process $e^+e^- \to t\bar{t}H$ in high energy e^+e^- colliders [14] and $\gamma\gamma \to t\bar{t}H$ in photon-photon colliders [15]. For large Higgs masses above the $t\bar{t}$ threshold, the decay channel $H \to t\bar{t}$ increases the cross section of $e^+e^- \to t\bar{t}Z$ through the reaction $e^+e^- \to ZH(\to t\bar{t})$ [33]; without the Higgs decay this final state is produced mainly through virtual γ and Z bosons.

We thus conclude that the essential elements of the profile of Higgs bosons in the intermediate mass range can be scanned very accurately at e^+e^- colliders.

ACKNOWLEDGMENTS

We enjoyed interesting conversations with K. Hagiwara and M. L. Stong on their discussion of the VVH coupling, which partly overlaps with our analysis. Helpful comments by J. F. Gunion are also gratefully acknowledged. This research was supported in part by the University of Wisconsin Research Committee with funds granted by the Wisconsin Alumni Research Foundation, in part by the U.S. Department of Energy under Contract No. DE-AC02-76ER00881, and in part by the Texas National Laboratory Research Commission under Grant No. RGFY93-221.

[1] P. W. Higgs, Phys. Rev. Lett. **12**, 132 (1964); Phys. Rev. **145**, 1156 (1966); F. Englert and R. Brout, Phys. Rev. Lett. **13**, 321 (1964); G. S. Guralnik, C. R. Hagen, and T. W. Kibble, *ibid.* **13**, 585 (1964).

[2] N. Cabibbo, L. Maiani, G. Parisi, and R. Petronzio, Nucl. Phys. **B158**, 295 (1979); M. Chanowitz, M. Furman, and I. Hinchliffe, Phys. Lett. **78B**, 285 (1978); R. A. Flores and M. Sher, Phys. Rev. D **27**, 1679 (1983); M. Lindner, Z. Phys. C **31**, 295 (1986).

[3] M. Sher, Phys. Rep. **179**, 273 (1989).

[4] D. Treille, talk at the Workshop on Physics and Experimentation with e^+e^- Linear Colliders, Waikoloa, Hawaii, 1993 (unpublished).

[5] J. Gunion *et al.*, in *Physics of the Superconducting Super Collider, Snowmass, 1986,* Proceedings of the Summer Study, Snowmass, Colorado, 1986, edited by R. Donaldson and J. Marx (Division of Particles and Fields of the APS, New York, 1987); R. M. Barnett, in *High Energy Physics in the 1990's*, Proceedings of the Summer Study, Snowmass, Colorado, 1988, edited by S. Jensen (World Scientific, Singapore, 1989); J. F. Gunion *et al.*, in *Research Directions for the Decade*, Proceedings of the Summer Study, Snowmass, Colorado, 1990, edited by E. L. Berger (World Scientific, Singapore, 1992), p. 59; D. Froidevaux *et al.*, in *Proceedings of the ECFA Large Hadron Collider Workshop,* Aachen, Germany, 1990, edited by G. Jarlskog and D. Rein (CERN Report No. 90-10, Geneva, Switzerland, 1990); G. Altarelli, *ibid.*; D. Denegri, *ibid.*

[6] *e^+e^- Colliders at 500 GeV: The Physics Potential*, Proceedings of the Munich-Annency-Hamburg Workshop, 1991, edited by P. M. Zerwas (DESY Report No. 92-123, Hamburg, Germany, 1992).

[7] D. R. T. Jones and S. T. Petcov, Phys. Lett. **84B**, 440 (1979); R. N. Cahn and S. Dawson, Phys. Lett. **136B**, 196 (1984); K. Hikasa, Phys. Lett. **164B**, 341 (1985); G. Altarelli, B. Mele, and F. Pitolli, Nucl. Phys. **B287**, 205 (1987).

[8] J. Ellis, M. K. Gaillard, and D. V. Nanopoulos, Nucl. Phys. **B106**, 292 (1976); J. D. Bjorken, in Proceedings of Summer Institute on Particle Physics (SLAC Report No. 198, 1976), p. 1; B. Ioffe and V. Khoze, Fiz. Elem. Chastits At. Yadra **9**, 118 (1978) [Sov. J. Part. Nucl. Phys. B **9**, 50 (1978)]; B. W. Lee, C. Quigg, and H. B. Thacker, Phys. Rev. D **16**, 1519 (1977).

[9] A. Djouadi, D. Haidt, B. Kniehl, B. Mele, and P. M. Zerwas, in *e^+e^- Colliders at 500 GeV: The Physics Potential* [6].

[10] P. Grosse-Wiesmann, D. Haidt, and J. Schreiber in Ref. [6].

[11] V. Barger, K. Cheung, B. A. Kniehl, and R. J. N. Phillips, Phys. Rev. D **46**, 3725 (1992).

[12] Z. Kunszt and W. J. Stirling, Phys. Lett. B **242**, 507 (1990); N. Brown, Z. Phys. C **49**, 657 (1991); V. Barger and K. Whisnant, Phys. Rev. D **43**, 1443 (1991).

[13] J. M. Cornwall, D. N. Levin, and G. Tiktopoulos, Phys. Rev. D **10**, 1145 (1974); M. S. Chanowitz and M. K. Gaillard, Nucl. Phys. **B261**, 379 (1985); H. Veltman, Phys. Rev. D **41**, 2294 (1990).

[14] A. Djouadi, J. Kalinowski, and P. M. Zerwas, Z. Phys. C **54**, 255 (1992).

[15] E. Boos *et al.*, Z. Phys. **C56**, 487 (1992); K. Cheung, Phys. Rev. D **47**, 3750 (1993).

[16] J. Fleischer and F. Jegerlehner, Nucl. Phys. **B216**, 469 (1983); B. A. Kniehl, Z. Phys. C **55**, 605 (1992); A. Denner, J. Küblbeck, R. Mertig, and M. Böhm, *ibid.* **56**, 261 (1992).

[17] T. Barklow, P. Chen, and W. Kozanecki, in *e^+e^- Colliders at 500 GeV: The Physics Potential* [6].

[18] V. Barger, T. Han, and R. J. Phillips, Phys. Rev. D **38**, 2766 (1988); V. Barger and T. Han, Mod. Phys. Lett. A **5**, 667 (1990).

[19] The relevant parameters are collected by J. Rossbach, Report No. DESY-M-93-1 (unpublished); P. M. Zerwas, in *Proceedings of the LC92 Workshop*, Garmisch-Partenkirchen, Germany, 1992, edited by R. Settles (DESY Report No. 93-001, Hamburg, in press).

[20] See the *High Luminosities at LEP*, Proceedings of the Workshop (CERN Report No. 91-02, Geneva, Switzerland, in press).

[21] J. Gunion, H. Haber, G. Kane, and S. Dawson, *The Higgs Hunter's Guide* (Addison-Wesley, Reading, 1990); A. Mendez and A. Pomerol, Phys. Lett. B **272**, 313 (1991); J. F. Gunion, H. E. Haber, and C. Kao, Phys. Rev. D **46**, 2907 (1992).

[22] M. J. Duncan, G. Kane, and W. Repko, Nucl. Phys. **B272**, 517 (1986); J. R. Dell' Aquila and C. A. Nelson, Phys. Rev. D **33**, 80 (1988); **33**, 93 (1988); **33**, 101 (1988); T. Matsuura and J. van der Bij, Z. Phys. C **51**, 259 (1991); H. Pois, T. J. Weiler, and

T. C. Yuan, Phys. Rev. D **47**, 3886 (1993); D. Chang, W. L. Keung, and I. Phillips, *ibid.* **48**, 3225 (1993).
[23] L. Resnick, M. K. Sundaresan, and P. J. S. Watson, Phys. Rev. D **8**, 172 (1973).
[24] B. A. Kniehl, Nucl. Phys. **B352**, 1 (1991).
[25] W.-Y. Keung and W. J. Marciano, Phys. Rev. D **30**, 248 (1984).
[26] J. R. Dell' Aquila and C. A. Nelson, Nucl. Phys. **B320**, 61 (1989).
[27] J. H. Kühn *et al.*, in *Z Physics at LEP 1*, Proceedings of the Workshop, Geneva, Switzerland, 1989, edited by G. Altarelli, R. Kleiss, and C. Verzegnassi (CERN Report No. 89-08, Geneva, 1989); G. Altarelli and B. Mele, Phys. Lett. B **299**, 345 (1993).
[28] N. P. Samios, R. Plano, A. Prodell, M. Schwartz, and J. Steinberger, Phys. Rev. Lett. **3**, 524 (1959).
[29] I. F. Ginzburg, G. L. Kotkin, S. L. Panfil, V. G. Serbo, and V. I. Telnov, Nucl. Instrum. Methods **219**, 5 (1984).
[30] B. Grzadkowski and J. F. Gunion, Phys. Lett. B **294**, 361 (1992); J. F. Gunion, talk at the Workshop on Physics and Experimentation with e^+e^- Linear Colliders [4].
[31] O. J. P. Eboli, M. C. Gonzales-Garcia, F. Halzen, and D. Zeppenfeld, Phys. Rev. D **48**, 1430 (1993).
[32] M. Hildreth, Report No. SLAC-PUB 6036 (unpublished).
[33] K. Hagiwara, H. Murayama, and I. Watanabe, Nucl. Phys. **B367**, 275 (1991).